Light and Strong SiC Networks

Claudio Ferraro, Esther Garcia-Tuñon, Victoria G. Rocha, Suelen Barg,
Maria Dolores Fariñas, Tomas E. Gomez Alvarez-Arenas, Giorgio Sernicola,
Finn Giuliani, and Eduardo Saiz*

The directional freezing of microfiber suspensions is used to assemble highly porous (porosities ranging between 92% and 98%) SiC networks. These networks exhibit a unique hierarchical architecture in which thin layers with honeycomb-like structure and internal strut length in the order of 1–10 µm in size are aligned with an interlayer spacing ranging between 15 and 50 µm. The resulting structures exhibit strengths (up to 3 MPa) and stiffness (up to 0.3 GPa) that are higher than aerogels of similar density and comparable to other ceramic microlattices fabricated by vapor deposition. Furthermore, this wet processing technique allows the fabrication of large-size samples that are stable at high temperature, with acoustic impedance that can be manipulated over one order of magnitude (0.03–0.3 MRayl), electrically conductive and with very low thermal conductivity. The approach can be extended to other ceramic materials and opens new opportunities for the fabrication of ultra-light structures with unique mechanical and functional properties in practical dimensions.

1. Introduction

In recent years, a significant effort has been devoted to the development of ultralight, highly porous ceramic structures. Their potential mechanical and functional capabilities are of interest in many advanced technologies from transportation to catalysis or tissue engineering.[1–6] To a large extent, the challenge for these applications is to attain large porosities (above 90%) while maintaining the pore size in the microscopic scale and retaining strength and structural capabilities. A range of

C. Ferraro, Dr. E. Garcia-Tuñon, Dr. V. G. Rocha,
G. Sernicola, Dr. F. Giuliani, Prof. E. Saiz
Centre for Advanced Structural Ceramics
Department of Materials
Imperial College London
South Kensington Campus
London SW7 2AZ, UK
E-mail: e.saiz@imperial.ac.uk

Dr. S. Barg
The School of Materials
The University of Manchester
Oxford Road, Manchester M13 9PL, UK

M. D. Fariñas, Dr. T. E. G. Alvarez-Arenas
Sensors and Ultrasonic Technologies Department
Information and Physics Technologies Institute (ITEFI)
Spanish National Research Council (CSIC)
Serrano 144, 28006 Madrid, Spain

highly porous ceramics have been fabricated in macroscopic dimensions using diverse technologies such as emulsification or direct foaming; however, the pore sizes are large (typically above 100 µm) and the materials tend to be weak.[5] At the other extreme, aerogels exhibit nanosized pores but are not strong.[7,8] Recent work has demonstrated the fabrication of metallic[9] and ceramic[1,3,4,6] microlattices with microsized pores and struts by combining additive manufacturing and thin film deposition. They can reach remarkable mechanical properties as a result of their carefully designed architectures but their dimensions are usually small (10–10^3 µm) and to date they have been fabricated from a very limited range of materials (Al$_2$O$_3$ and TiN).[1,3,4,6] The challenge remains on how to broaden the material palette to form strong, thermally and chemically stable light structures in practical dimensions using flexible, low-cost technologies for high-volume fabrication.

Silicon carbide is a very appealing material for the fabrication of light structures and microlattices. It combines excellent thermal stability and shock resistance, low thermal expansion, superb mechanical strength, and high chemical stability.[10,11] As a consequence, light and porous SiC structures are of interest for a number of advanced technological applications. Commercial uses of porous silicon carbide have already been exploited for example in filters for water, diesel particulate, hot gas or molten metals, porous burners, metal and polymer matrix composites, high-temperature/high-voltage semiconductor electronics, or membranes.[11] However, these are "conventional" porous materials with porosities still below 80%. The development of even lighter, stiff and strong porous SiC would be extremely advantageous for many of these technologies and would open new opportunities in others.

Nature offers many examples of highly porous materials (such as bone or wood) that are light and retain toughness and strength. A common characteristic of these biological materials is their complex hierarchical architecture from the macro down to the nanoscale.[12] It has been also shown how the architecture of lattices can be manipulated to create stretching-dominated structures and increase their mechanical efficiency.[6,13] However, when translating these structural concepts, it is important to remember that the strength and stiffness of a porous ceramic scale with those of their wall or strut.

These should be free of microdefects to enhance mechanical performance.[14] In consequence, a very appealing way to create a strong, highly porous ceramic lattice is through the controlled assembly of thin, strong microfibers into complex hierarchical architectures. The assembly of complex, highly porous macroscopic structures from microfibers remains a challenge.[15] Here we address it by directionally freezing suspensions of SiC fibers to assemble ceramic networks with macroscopic dimensions, porosities above 90% and densities below 300 mg cm^{-3}. This approach allows the formation of lattices with layered architectures that can be manipulated by controlling the composition of the suspension and the freezing conditions. The use of SiC enables the fabrication of light structures that retain strength and stiffness and are stable up to high temperatures. Their pore and strut sizes along with their mechanical properties are comparable to microlattices prepared through thin film deposition and they exhibit a unique combination of properties: they are electrically conductive, thermally insulating, and present very low acoustic impedance. The effect of the processing conditions on the architecture is evaluated and the mechanical and thermal properties of the networks are compared with other ceramic materials of similar densities and with existing models.

2. Results

Freeze casting of ceramics is based on the directional freezing of a suspension. As the ice grows it expels the ceramic particles that accumulate in the space between ice crystals (**Figure 1**). After sublimating the water is possible to obtain a porous ceramic whose porosity has been templated by the ice. In order to obtain a homogeneous structure the suspension should remain stable during freezing. However, due to their dimensions (diameter ≈1.5 μm, average length of ≈18 μm) the SiC fibers can sediment rapidly resulting in inhomogeneous materials. To avoid this problem, chitosan was used to prepare homogeneous and stable slurries. The hydroxyl and amine groups present in the repeating unit of the chitosan chain interact with the silanol groups formed on the SiC surface in the presence of water through hydrogen bonding.[16] These interactions along with the electrostatic forces between the chitosan chains and the SiC surfaces result in weakly flocculated suspensions. Flocculation hampers sedimentation enabling the formation of homogeneous structures. By directionally freezing the suspension, we promote the formation of lamellar ice that expels the fibers as it grows. Although flocculation due to chitosan increases the viscosity, it remains low enough to allow the formation of large, lamellar ice crystals (the apparent viscosity is well below 100 Pa s for fiber contents up to 20 wt%). As the fibers pack in the layers between the growing ice crystals they form a microporous network (Figure 1). After removing the ice template via freeze drying, we obtain a highly porous network (an irregular microlattice) with a layered architecture and macroscopic dimensions (sizes up to centimeters).

After drying, the sample is thermally treated to sinter the individual fibers and consolidate the structure. Sintering takes place in a graphite furnace at 1800 °C under argon flow. To promote pressureless sintering Al_2O_3 and Y_2O_3 are added to the slurry (up to 15 wt% of the SiC content).[17] These additives in combination with the silica present on the SiC surface promote the formation of liquid at high temperature. The liquid phase enhances mass transport and facilitates fiber–fiber bonding (Figure 1d). To achieve this goal and avoid the evaporation of additives at high temperature a tight control of the atmosphere is maintained by placing the sample in a closed graphite crucible, on a SiC/Al_2O_3 powder bed. Chitosan is also expelled from the growing ice crystals during freezing and subsequently eliminated during sintering.[18] The sintered lattices exhibit a structure with highly interconnected porosity and a hierarchical architecture (Figure 1) formed by aligned, thin and highly porous ceramic layers. The SiC fibers form the network struts and the architecture can be manipulated by controlling the freezing conditions and the composition of the suspension. In particular, the final density of the material is determined by the solid concentration in the suspension and the distance between layers by the speed of the ice front and also the solid concentration. This separation can vary between 15 and 50 μm. As it has been observed in other systems, faster speeds result in smaller interlayer distances.[19] The wall thickness remains constant and of the order of the fiber diameter (Figure 1b). The length of the struts inside the walls varies between 1 and 10 μm. By reducing the solid loading of the suspension from 7 to 1.5 vol%, the porosity increases from 92% up to 98%. Some fibers are trapped by the growing ice crystals during freezing and arrange perpendicularly to the lamellae forming bridges between them (Figure 1d). The number of bridges increases with increasing fiber concentration in the starting suspensions and as a result the structure of denser lattices transitions toward a more isotropic, cellular architecture (Figure 1).

The combination of high porosity with the intrinsic properties of SiC results on the formation of structures that are both electrically conductive (conductivities ranging from 5.3×10^{-6} to 3.8×10^{-4} S cm^{-1}) and thermally insulating (thermal conductivities of the order of 0.1–0.6 W m^{-1} K^{-1}). There is a slight dependence of the thermal conductivity with the orientation for samples with higher porosity (**Figure 2**). This anisotropy could also be observed in the electrical conductivity that can be between two and six times larger in the direction parallel to the layers. Conductivity is approximately three times larger in the direction parallel to the layers for samples with a porosity of 97%. During the measurements the samples remained stable up to 1500 °C. The thermal conductivity also remained relatively stable (although it increases slightly for samples with larger pores).

The structures fail in a brittle manner under compression. As it is usually observed in brittle porous materials, the stress/strain curve reaches a plateau.[14] In this plateau, it is possible to observe dips corresponding to failure events. However, the strength is recovered after each dip (**Figure 3**). The in situ mechanical tests in the scanning electron microscopy (SEM) revealed that when the scaffolds reach their crushing strength, the junctions between fibers at the top and the bottom of the lattice (in contact with the plates of the testing machine) start to break and the fibers accumulate (Figure 3). Wall failure at the top or bottom of the sample causes the observed dips in stress at the plateau. However, the bulk of the structure remains stable and
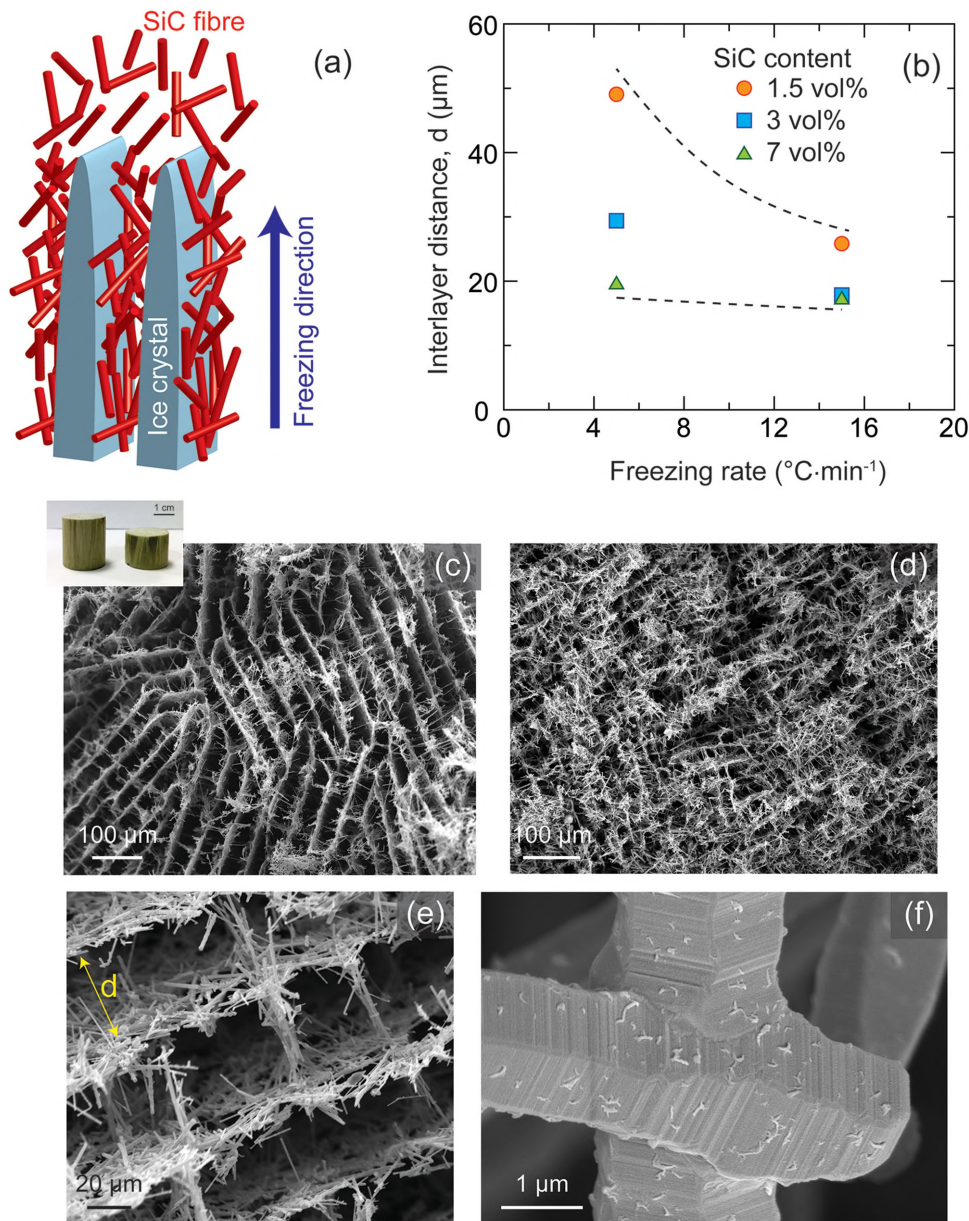
Figure 1. a) Schematic of the freeze casting process. Lamellar ice crystals grow directionally in a fiber water-based suspension frozen under a temperature gradient. The fibers are expelled from the growing ice and form a layered structure. b) The interlayer distance, *d*, decreases when increasing the speed of the ice front and increasing the solid content of the suspension. c) Scanning electron image showing the layered structure of a sintered network prepared using a suspension containing 1.5 vol% fibers (98% final porosity). The inset shows how it is possible to prepare structures with macroscopic dimensions. d) Networks sintered from a 7 vol% fiber suspension (92% final porosity) showing a more isotropic structure. e) Detail of the structure shown in (c). The walls are thin (1–2 μm) and formed by entangled fibers. Some fibers arrange perpendicular to the walls forming bridges between them. f) Junction between fibers showing some of the remaining liquid phase formed during sintering.

is still able to sustain the applied load. This type of behavior has been observed in other porous ceramics and microlattices.[4,23]

Anisotropy is observed in the velocity of propagation of ultrasonic waves (**Figure 4**). In the direction parallel to the layers they propagate between 15% and 35% faster than along the normal direction (anisotropy increases with decreasing density). As expected, the ultrasound wave velocity takes very low values that increase with sample density (from 340 to 540 m s^{-1} for 100 mg cm^{-3}, up to 1100–1400 m s^{-1} for 250 mg cm^{-3}).

Velocity values in the low range are similar to those measured in silica aerogels with a similar technique. In addition, acoustic impedance can be very small (down to 0.03 MRayl) and the ultrasound attenuation coefficient is relatively low (50–60 Np m^{-1} @ 300 kHz), these values are similar to those found in conventional silica aerogels.[24] Moreover, changing the density makes possible to vary the impedance values over one order of magnitude (0.03–0.3 MRayl). This makes this kind of material a suitable candidate to produce stacks of impedance
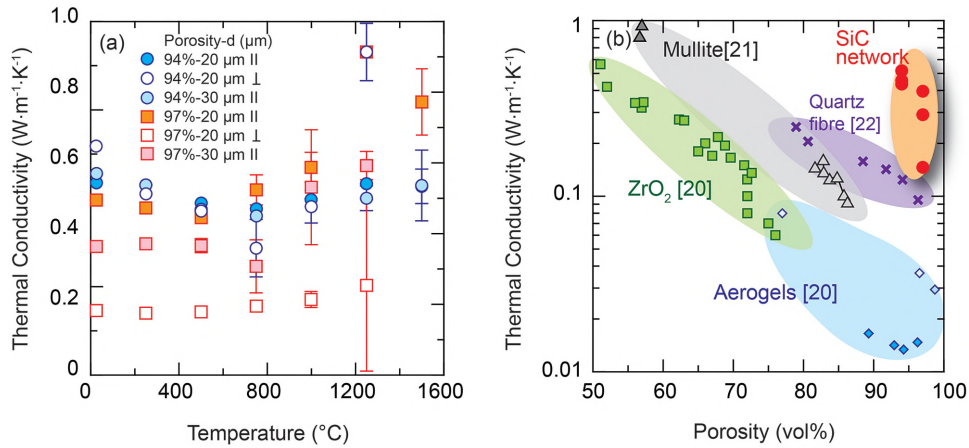
Figure 2. a) The thermal conductivities in the direction parallel (II) and perpendicular (⊥) to the layers remain low with temperature up to 1500 °C although it tends to increase at higher temperatures for the materials with larger pores. b) The thermal conductivity (room temperature values) of the SiC networks is comparable to other porous thermally insulating ceramics. Aerogels have lower thermal conductivity and are lighter but they are also weaker (data from refs. [20–22]).

matching layers for wide-band air-coupled piezoelectric transducers in the low megahertz frequency range or for the realization of acoustic metamaterials.[25] There they could substitute other very low density materials (aerogels) but offering much better machinability and mechanical stability.

3. Discussion

The mechanical properties of a lattice depend on its architecture and the strength and modulus of the struts. In ceramic microlattices fabricated by additive manufacturing and thin
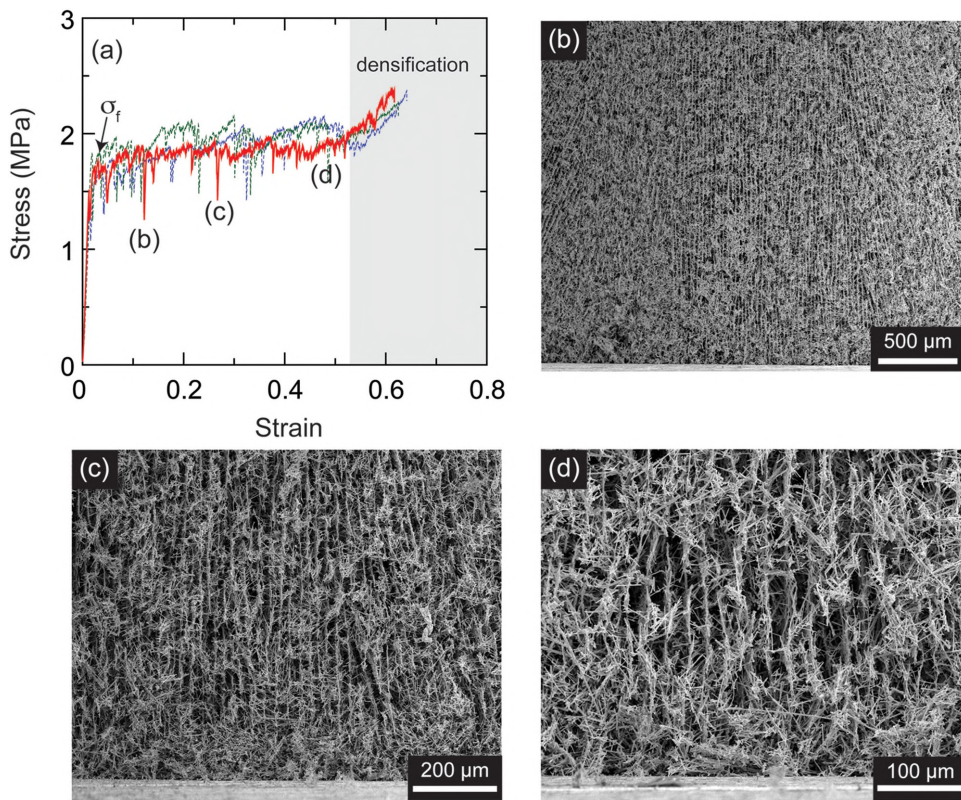

Figure 3. a) Stress–strain curves showing the brittle fracture behavior of lattices with a porosity of 94%. After reaching the compressive strength (σ_f) the curve exhibits a plateau with dips in stress corresponding to failure events followed by a fast increase due to densification. b–d) The sequence of pictures taken "in situ" in the SEM (corresponding to the continuous red line) shows how failure occurs at the junction between fibers at the top and bottom of the sample while the center remains intact and can still hold the load. The sample can still sustain load even after a strain above 40%.
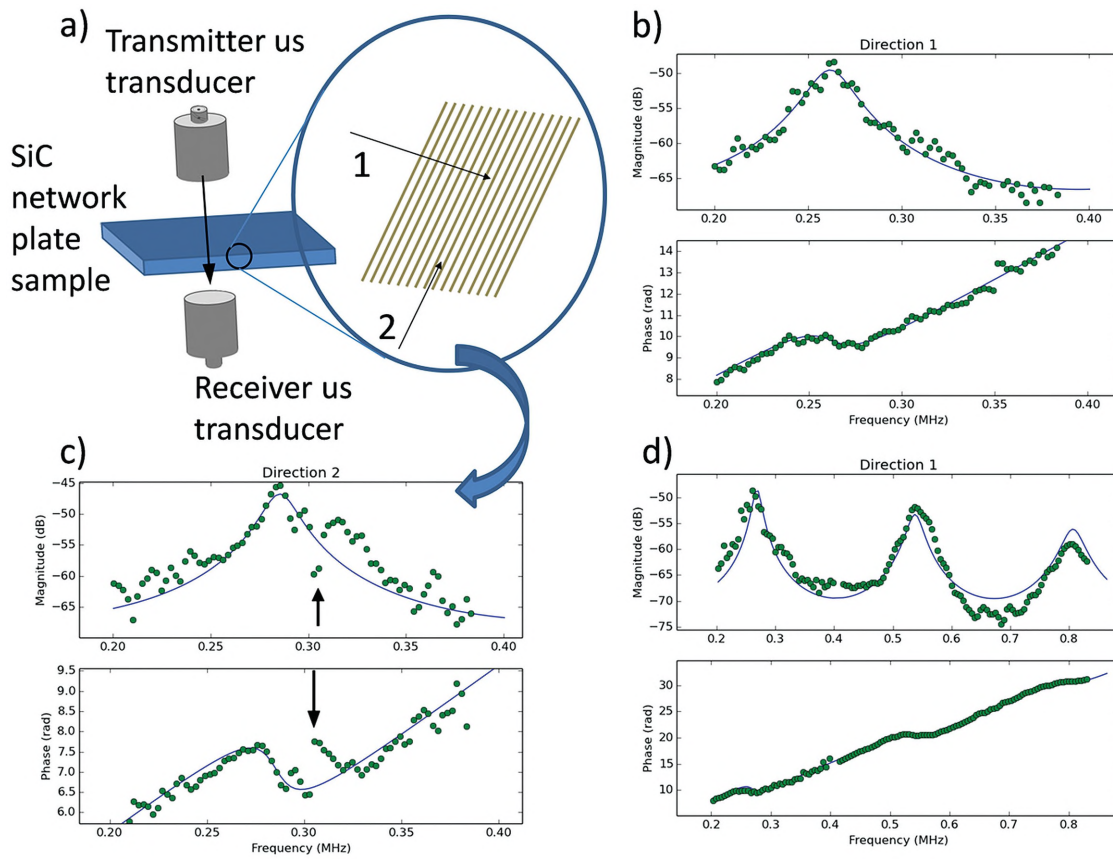
Figure 4. a) Schematic representation of the experimental set-up to measure thickness resonances in the transmission coefficient of plates at normal incidence showing transmitter and receiver ultrasonic (us) transducers; and the two main directions of propagation of the ultrasonic waves in the material: along the layered microstructure and normal to it. b,c) Dots: Measured magnitude and phase spectra of the first thickness resonance of the plate for plates cut along the two main directions in the material (sample 20%, 0.2 g cm^{-3}); solid line: calculated response assuming the plate as an homogenous material. While for propagation along direction 1 (plate thickness 2.6 mm) the material exhibit a behavior very close to the expected one for an homogeneous material, along the direction 2 (plate thickness 1.9 mm) a sharp interference is always observed that produces a remarkable distortion of the spectra of the first thickness resonance (in the case shown, at 310 kHz, see arrows). This interference can be explained by the appearance of two different guided waves that propagate along the two different and simultaneous paths of propagation that the material offers in this direction: along the layers and along the spaces between them. d) Dots: Measured magnitude and phase of the first three orders of the thickness resonances for wave propagation in the direction 1; solid line: calculated response assuming the plate as a homogenous material. For this direction, material behaves as an homogeneous material in a very wide frequency band; on the contrary, for propagation in the direction 2 the spectra become distorted as frequency increases and no higher order resonances are observed.

film deposition the defect size is limited by the very thin strut walls (typically ≈10 nm thick). In consequence they can exhibit very high specific strengths. In addition, their geometries can be designed to avoid strut bending during compression and achieve a more efficient relationship between mechanical response (strength and stiffness) and density. However, the processing approach limits the dimension of the lattice to few millimeters at most.

Here we address this problem using a bottom up fabrication approach to assemble strong microscopic ceramic fibers into macroscopic (centimeters in size) structures. The bending strength of the fibers has been measured in situ in the scanning electron microscope using three-point bending. They reach values of the order of 1–3 GPa, much larger than those usually reported for sintered ceramics and comparable to those estimated for the struts of ceramic microlattices (**Figure 5**).[3,4] Although the three-point bending tests could be overestimating

slightly the fracture strength we take this as a good indicative value for the following calculations.

The fibers assemble into walls aligned parallel to the direction of ice growth. Because fiber assembly is not very efficient the walls are formed by a highly porous fiber network. This assembly process results in materials that are clearly orthotropic. The two dimensions perpendicular to the freezing direction show similar properties compared to the third direction parallel to the freezing path. Due to the combination of strong SiC struts with a layered structure, the materials exhibit high crushing strengths and Young's modulus in the freezing direction (parallel to the walls) even at low densities (**Figure 6**). The measured values are significantly higher than aerogels and comparable to microscopic ceramic lattices with similar densities fabricated using vapor deposition.

The effect of fiber strength and lattice architecture can be discussed by comparing the expected theoretical strength and
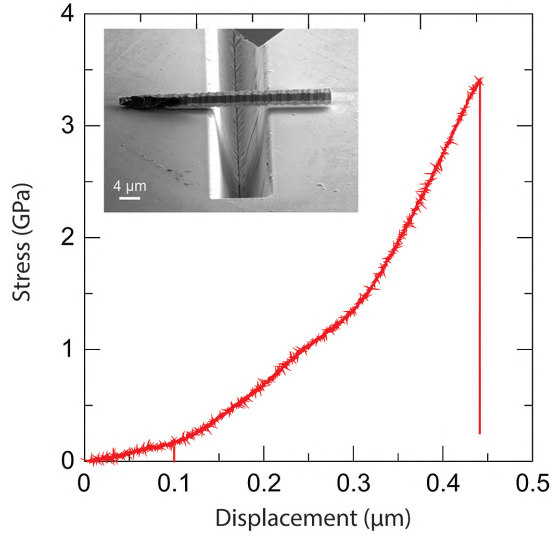
Figure 5. Stress/strain curve from a single fiber bending test performed in situ in the scanning electron microscope (inset is a scanning electron microscopy showing the set-up). The initial nonlinearity of the curve is likely due to fiber movement under the indenter.

stiffness of the structures with our experimental results. The material could be model as a set of parallel honeycombs (in our case, the walls formed through fiber assembly) where the separation between honeycombs is determined by the freezing conditions. To simplify the discussion, if we considered a regular hexagonal honeycomb whose deformation is determined by bending of the struts, the strength, σ_h, and Young modulus, E_h, of the wall in the freezing direction could be written as[14]

$$E_h = 2.3 E_{SiC} \left(\frac{t}{l} \right)^3 \tag{1}$$

$$\sigma_h = \frac{4}{9} \sigma_{SiC} \left(\frac{t}{l} \right)^2 \tag{2}$$

where E_{SiC} and σ_{SiC} are the Young modulus and strength of the SiC fibers, t is their diameter, and l is the side length of the hexagons. The ratio t/l will determine the density, ρ_h, of the honeycomb (the wall in our case). If we consider that the density of the fibers is the density of SiC, ρ_{SiC}, then the wall density is

$$\rho_h = \rho_{SiC} \frac{2}{\sqrt{3}} \frac{t}{l} \tag{3}$$

The properties of the structure (density, ρ, modulus, E, and strength, σ) scale with those of the wall as $\approx w/(w+d)$ where w is the wall thickness (of the order of t) and d the interlayer distance (Figure 1d). As a result $E \propto \rho^3$ and $\sigma \propto \rho^2$. This could be compared to the predictions for an isotropic lattice

$$E \approx E_f \left(\frac{\rho}{\rho_{SiC}} \right)^2 \tag{4}$$

$$\sigma \approx 0.2 \sigma_f \left(\frac{\rho}{\rho_{SiC}} \right)^{\frac{3}{2}} \tag{5}$$

It is important to remember that these equations describe a bend-dominated scaling. For a deformation dominated by stretching the modulus and strength will vary linearly with density.[13,26] When comparing the different theoretical expectations (dashed lines in Figure 6) it can be observed that, for lattices working in a bending mode, a layered structure with the wall to pore width ratio of our networks is more efficient than the isotropic one (when compression takes place in the direction parallel to the layers). Furthermore for porosities below ≈95% the layered design is also more efficient that an isotropic design working in the stretching mode (Figure 6c,d).

The experimental strengths are of the order of those measured for regular microlattices but lower than the predictions (dashed lines in Figure 6). This can be mostly attributed to the fact that failure occurs at the junction between fibers that seems to be a "weak" spot as it has been observed in the in situ tests (Figure 3). Finite element simulations have shown how maximum stresses in macro and microlattices tend to happen at the junctions during compression.[3,28] Strength and stiffness scale with density following a power law very close to what could be expected from Equations (1) and (2) (≈3 and 1.9, respectively). These results suggest that the model of parallel honeycombs with bend-dominated deformation describes the system relatively well. Still, it has to be considered that the model is an oversimplification and there is a transition toward a more isotropic lattice as the solid content in the suspension increases and the number of interlayer bridges grows. In addition the formation fiber bundles may also diminish the properties (in particular the modulus). This effect may be more evident as the densities of the samples increase. Finally it should be emphasized that the efficiency of the layered structure is very dependent of the ratio between the pore width and the wall thickness. In our structures it remains more or less constant (slower cooling rates result in wider pores but also in thicker walls). However, for two layered structures with same relative density, if the thickness of the wall remains constant, increasing the pore width results in a weaker, less-stiff structure.

The mechanical properties are closer to those of very light polymer foams or wood than to porous ceramics (**Figure 7**). As expected, the low densities result in ultrasound propagation velocities that are comparable to aerogels and other highly porous natural materials such as cork. These structures show a unique combination of low thermal conductivity and low electrical resistivity (Figure 7). The thermal conductivities are at least one order of magnitude lower than those of conventional SiC foams with porosities below 80%.[29] By manipulating the architecture and decreasing the density is it possible to create a structure with a thermal conductivity comparable to some of the well-known porous ceramic and fiber glass insulating systems using a ceramic with a relatively high thermal conductivity (Figure 2). The relative decrease in conductivity (the one of the porous structure vs that of the dense material) is significantly lower than for other porous ceramic systems while similar specific strengths are retained (Figure 7c) what points to an interesting direction for the design and fabrication of novel
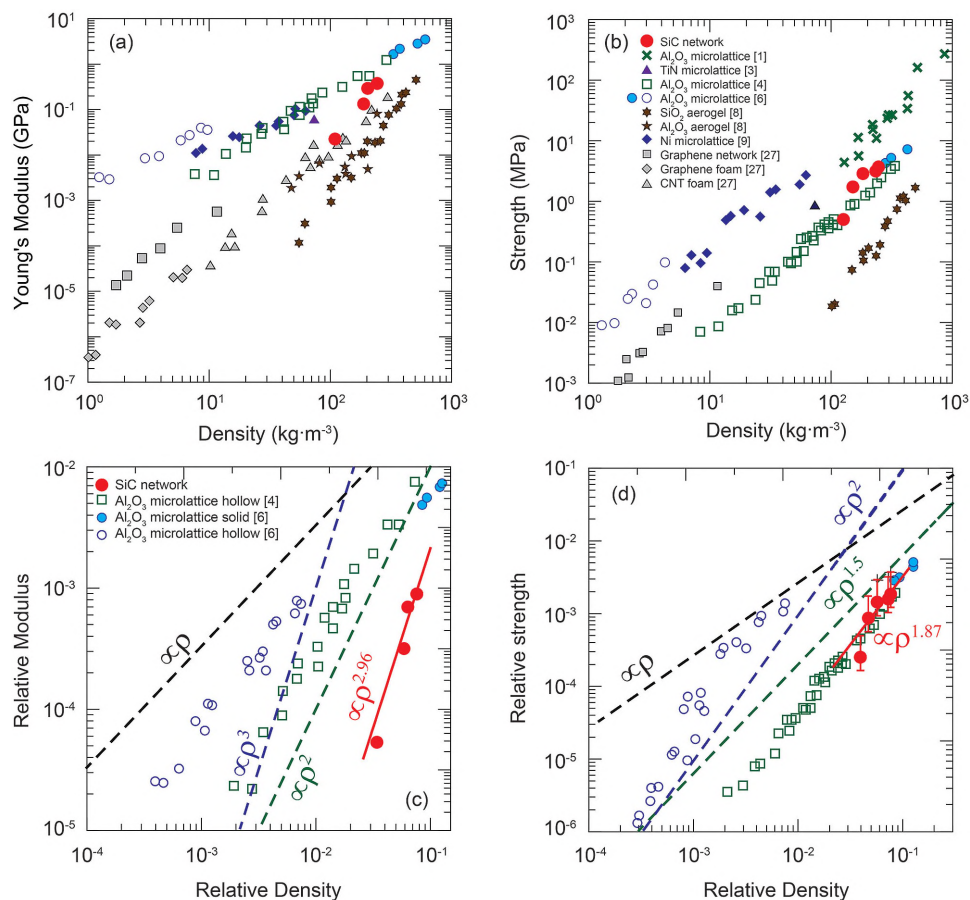
Figure 6. Mechanical properties of the SiC networks. a) Comparison of the Young's modulus of the SiC networks with other ultralight inorganic materials. b) Comparison of the crushing strength. c) Relative Young modulus (E/E_f) as a function of the relative density for ceramic microlattices. d) Relative strength (σ/σ_f). In (c) and (d) theoretical predictions for layered and isotropic lattices (Equations (1)–(5)) are plotted for comparison (dashed lines). In order to calculate the relative strength and toughness for the data in ref. [4], a Young modulus of 164 GPa and a strength of 2 GPa were used following the values given in the reference. When using a layered model, we have assumed $(w + d)/d = 26$ according to the microstructural observations. The stiffness and strength of the freeze casted network is above that of aerogels. The strengths are in the range of those measured for microlattices prepared through the combination of additive manufacturing and thin film deposition. The stiffness is also comparable although in the lower range. The relative Young's modulus and strengths of the porous SiC structures have been calculated using $E_{SiC} = 450$ GPa and $\sigma_{SiC} = 2$ GPa (according to the fiber bending tests). Data are taken from refs. [1,3,4,6,8,9], and [27].

thermally insulating materials. Anisotropy decreases when increasing density due to a transition to a more cellular structure as more fiber bridges form between the walls. Although silica aerogels are substantially better thermal insulators they are significantly weaker and electrically insulating. In addition, the networks produced in this work remain stable with low thermal conductivity at temperatures up to 1500 °C that is far higher than usually achieved with other porous thermal insulating ceramics.[22] The small increase in thermal conductivity with temperature for samples with larger pores could be attributed to the radiative component of the thermal conductivity. Overall, the transport properties (sound propagation, thermal, or electrical conductivity) reflect the anisotropic structure of the material. In the direction parallel to the layers there are two "competing" paths, the SiC walls formed by tangled fibers and the gas between them. Transport is faster along the walls and, as expected, increases with density (as the wall gets denser it favors better conductivity). In the direction perpendicular to the walls sound and thermal transport occurs by "jumping"

from one media to the other (from wall to gas phase and so on) while electrical conductivity depends on the existence of fibers bridging the walls. As a result transport properties are diminished.

4. Conclusion

In summary, we are able to produce ultralight SiC structures with macroscopic dimensions and microscopic porosity through a wet processing technique. These structures exhibit a combination of low density and mechanical strength comparable to microlattices fabricated through lithography and vapor deposition. Although they still deform in a bending-dominated mode, a layered architecture combined with strong SiC struts provides strengths and stiffness comparable to microlattices designed to work in a stretching dominated regime. The SiC networks also exhibit a unique combination of functional properties such as low acoustic impedance, thermal stability,
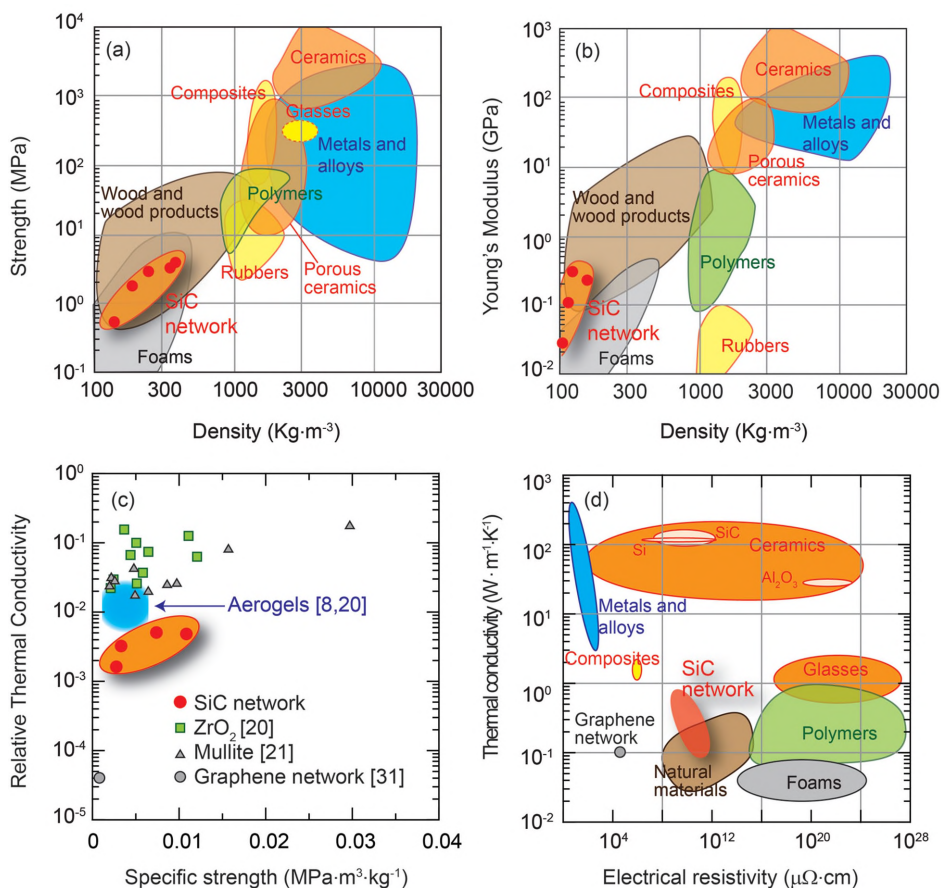
Figure 7. a) Strength and b) Young modulus of the SiC networks compared to other families of materials. The properties are closer to foams or wood than to conventional porous ceramics (graphs redrawn from ref. [30]). c) The hierarchical, highly porous structure of the SiC networks allows a very high decrease of the thermal conductivity compared with the dense material while maintaining a relatively high specific strength. d) When compared to other materials, the networks offer a unique combination of relatively high electrical conductivity (for a ceramic, comparable to Si or dense SiC) with low thermal conductivity (materials' data from ref. [30]). The following values have been used for the thermal conductivities of dense ceramics (SiO$_2$: 1.4 W m^{-1} K^{-1}; SiC: 90 W m^{-1} K^{-1}; mullite: 5 W m^{-1} K^{-1}, ZrO$_2$: 2.7 W m^{-1} K^{-1}; graphene: 2500 W m^{-1} K^{-1}).[21,31]

thermal insulation, and electrical conductivity. The use of wet processing allows the fabrication of these structures with different shapes and the technique can be scaled to prepare structures in practical dimensions. Because the process if based on a physical phenomenon (freezing), it could be extended to other ceramic fibers. In this example, the combination of the SiC properties with the structural manipulation by freeze casting makes these highly porous structures promising candidates in thermal or acoustic management, filters and catalyst supports designed to work at elevated temperatures or even as ceramic reinforcement in the production of composites.

5. Experimental Section

Starting Materials and Processing: Colloidal suspensions of SiC fibers were prepared by mixing 1.5, 3, and 7 vol% SiC fibers (Alfa Aesar) with a diameter of ≈1.5 μm and length of ≈18 μm. Chitosan solutions (1 wt%) were prepared by dissolving chitosan flakes (Sigma-Aldrich) (0.5 g) in 50 mL of an aqueous solution of acetic acid (Sigma-Aldrich, Reagent Plus, ≥99%) (0.05 M). SiC fibers were added to the chitosan suspension, ultrasonicated for 30 min and mixed for 24 h. Along with the SiC fibers,

15 wt% (with respect to the SiC) of Al$_2$O$_3$ (Baikalox B-series SMA6, Baikowski, France) and Y$_2$O$_3$ (Grade C-ABCR—H. C. Starck) were added to promote sintering. After mixing for 24 h, the suspensions were deaired for at least 30 min to remove air bubbles and frozen directionally by placing them on a Cu cold finger whose temperature was decreased at a constant rate of 15 K min^{-1}.[32] The frozen scaffolds were dried for 24 h (Freezone 4.5 by Labconco, USA) and subsequently sintered in an inert atmosphere (Ar) with a heating rate of 20 °C min^{-1} up to the maximum temperature (1800 °C); cooling rates were fixed at 20 °C min^{-1}.

Characterization: The apparent density and porosity of the sintered scaffolds were measured by Archimedes' method (Sartorius, YDK01, Goettingen, Germany) in water. The flow and viscoelastic properties of SiC fibers suspensions were measured in a Discovery Hybrid Rheometer HR1 (TA Instruments). The flow experiments were carried out with a parallel plate (∅ = 40 mm) with a solvent trap cover to prevent solvent evaporation under steady sensing. The microstructure of the materials was analyzed via SEM (Leo Gemini 1525). The flexural strength of single fibers was measured by in situ micro three point bending test. The fiber was placed on a trough, which edges were acting as supports, previously milled via focused ion beam on a silicon substrate. The fiber was loaded using an Alemnis nanoindenter equipped with a Synton-MDP diamond wedge tip moved in displacement control. The Alemnis was setup to displace the tip at a speed of 2 nm s^{-1} until failure of the fiber. The load was recorded by a Honeywell 50 g load cell sitting under the specimen

stub. The test was conducted in an Auriga Zeiss SEM; high resolution live images allowed a fine alignment of the tip over the specimen and a video of the test was recorded for further offline analysis. Compression tests were performed on a universal testing machine (Zwick/Roell 1474) with a load range up to 100 kN. The compression test was done following the ASTM C133-94 standard with a crosshead speed of 1.3 mm min^{-1}. In order to homogeneously distribute the load during the compression tests, a stainless steel semi sphere was placed at the top of the samples. For each composition, five to ten specimens measuring $\approx 5 \times 5 \times 5$ mm^3 were cut from a ceramic part with a diamond disk and grinded to ensure parallel surfaces. Elastic moduli were evaluated from the measurement of the ultrasonic phase velocity in the samples in the frequency range 0.1–0.9 MHz assuming a Poisson ratio of 0.3. To preserve the integrity of the sample and avoid introducing any modification in their response, we only used air-coupled ultrasonic techniques avoiding the use of coupling fluids between transducers and samples and/or any direct contact between them. Two different air-coupled ultrasonic techniques were used depending on the sample size, both operating in through transmission mode and at normal incidence. In both cases, wide-band and high sensitive piezoelectric air-coupled transducers[33] a PANAMETRICS 5077 pulser/receiver and a DPO5054 Tektronix oscilloscope were used. First, ultrasound velocity in $20 \times 20 \times 20$ mm^3 samples was obtained from conventional time of flight measurements in the three main directions. Afterward slices of dimensions of $\approx 20 \times 20 \times 1$ mm^3 were cut along the three main directions to test them in resonance to get a resonant frequency of the slice thickness mode about 0.25 MHz following the method explained by Alvarez-Arenas.[34]

Ultrasound velocity (v) is related with the density (ρ), bulk (K), and shear modulus (G), or Young modulus (E) and the Poisson ration (v)

$$v = \sqrt{\frac{K + \frac{4}{3}G}{\rho}} = \sqrt{\frac{E(1-v)}{(1+v)(1-2v)}} = \sqrt{\frac{G(4G-E)}{3G-E}} \quad (6)$$

The thermal properties of the samples were measured using a Nezstch LFA 427—Laser Flash Apparatus, at temperatures between 30 and 1500 °C. A short energy pulse heated up the bottom surface of the sample, while the temperature on the upper surface was measured and monitored with an infrared detector. The thermal diffusivity was measured in Ar atmosphere, using a heating rate of 10 °C min^{-1}. Between three and five measurements for each temperature were carried out. The "Cowan + pulse correction" diffusivity model was used for the processing of the experimental data. The thermal conductivities were calculated with Proteus Software, using the acquired data of thermal diffusivity, specific heat, and density of the samples. The electrical conductivity was measured as the inverse of the resistivity obtained with the two point technique

$$\rho = \frac{Rwh}{l} \quad (7)$$

where w, h, and l are the dimensions of the bars used for the test ($10 \times 10 \times 10$ mm^3). Copper contacts and silver paint were used to improve the electrical contact between the samples and the anodes.

Acknowledgements

[1] J. Bauer, S. Hengsbach, I. Tesari, R. Schwaiger, O. Kraft, *Proc. Natl. Acad. Sci. USA* **2014**, *111*, 2453.

[2] a) P. Colombo, *Science* **2008**, *322*, 381; b) J. Fricke, A. Emmerling, *Adv. Mater.* **1991**, *3*, 504; c) E. Garcia-Tunon, S. Barg, R. Bell, J. V. M. Weaver, C. Walter, L. Goyos, E. Saiz, *Angew. Chem. Int. Ed.* **2013**, *52*, 7805; d) U. T. Gonzenbach, A. R. Studart, E. Tervoort, L. J. Gauckler, *Angew. Chem. Int. Ed.* **2006**, *45*, 3526; e) U. T. Gonzenbach, A. R. Studart, E. Tervoort, L. J. Gauckler, *J. Am. Ceram. Soc.* **2007**, *90*, 16; f) A. R. Studart, U. T. Gonzenbach, I. Akartuna, E. Tervoort, L. J. Gauckler, *J. Mater. Chem.* **2007**, *17*, 3283.

[3] D. C. Jang, L. R. Meza, F. Greer, J. R. Greer, *Nat. Mater.* **2013**, *12*, 893.

[4] L. R. Meza, S. Das, J. R. Greer, *Science* **2014**, *345*, 1322.

[5] A. R. Studart, U. T. Gonzenbach, E. Tervoort, L. J. Gauckler, *J. Am. Ceram. Soc.* **2006**, *89*, 1771.

[6] X. Y. Zheng, H. Lee, T. H. Weisgraber, M. Shusteff, J. DeOtte, E. B. Duoss, J. D. Kuntz, M. M. Biener, Q. Ge, J. A. Jackson, S. O. Kucheyev, N. X. Fang, C. M. Spadaccini, *Science* **2014**, *344*, 1373.

[7] S. J. Teichner, G. A. Nicolaon, M. A. Vicarini, G. E. E. Gardes, *Adv. Colloid Interface Sci.* **1976**, *5*, 245.

[8] a) S. O. Kucheyev, T. F. Baumann, C. A. Cox, Y. M. Wang, J. H. Satcher, A. V. Hamza, J. E. Bradby, *Appl. Phys. Lett.* **2006**, *89*, 041911; b) T. Woignier, J. Reynes, A. H. Alaoui, I. Beurroies, J. Phalippou, *J. Non-Cryst. Solids* **1998**, *241*, 45.

[9] T. A. Schaedler, A. J. Jacobsen, A. Torrents, A. E. Sorensen, J. Lian, J. R. Greer, L. Valdevit, W. B. Carter, *Science* **2011**, *334*, 962.

[10] P. de Wit, E. J. Kappert, T. Lohaus, M. Wessling, A. Nijmeijer, N. E. Benes, *J. Membr. Sci.* **2015**, *475*, 480.

[11] J.-H. Eom, Y.-W. Kim, S. Raju, *J. Asian Ceram. Soc.* **2013**, *1*, 220.

[12] U. G. K. Wegst, H. Bai, E. Saiz, A. P. Tomsia, R. O. Ritchie, *Nat. Mater.* **2015**, *14*, 23.

[13] N. A. Fleck, V. S. Deshpande, M. F. Ashby, *Proc. R. Soc. A* **2010**, *466*, 2495.

[14] L. J. Gibson, M. F. Ashby, *Cellular Solids: Structure and Properties*, Cambridge University Press, Cambridge, UK **1997**.

[15] H. X. Peng, Z. Fan, J. R. G. Evans, *J. Mater. Sci.* **2001**, *36*, 1007.

[16] L. Saravanan, S. Subramanian, A. B. V. Kumar, R. N. Tharanathan, *Ceram. Int.* **2006**, *32*, 637.

[17] V. V. Pujar, R. P. Jensen, N. P. Padture, *J. Mater. Sci. Lett.* **2000**, *19*, 1011.

[18] a) N. L. Francis, P. M. Hunger, A. E. Donius, B. W. Riblett, A. Zavaliangos, U. G. K. Wegst, M. A. Wheatley, *J. Biomed. Mater. Res. A* **2013**, *101*, 3493; b) M. C. Gutierrez, M. J. Hortiguela, J. M. Amarilla, R. Jimenez, M. L. Ferrer, F. del Monte, *J. Phys. Chem. C* **2007**, *111*, 5557.

[19] C. Walter, S. Barg, N. Ni, R. C. Maher, E. Garcia-Tunon, M. M. Z. Ismail, F. Babot, E. Saiz, *J. Eur. Ceram. Soc.* **2013**, *33*, 2365.

[20] a) L. L. Gong, Y. H. Wang, X. D. Cheng, R. F. Zhang, H. P. Zhang, *J. Porous Mater.* **2014**, *21*, 15; b) B. Nait-Ali, K. Haberko, H. Vesteghem, J. Absi, D. S. Smith, *J. Eur. Ceram. Soc.* **2006**, *26*, 3567; c) J. Fricke, X. Lu, P. Wang, D. Buttner, U. Heinemann, *Int. J. Heat Mass Transfer* **1992**, *35*, 2305; d) T. Y. Wei, T. F. Chang, S. Y. Lu, Y. C. Chang, *J. Am. Ceram. Soc.* **2007**, *90*, 2003.

[21] a) R. Barea, M. I. Osendi, J. M. F. Ferreira, P. Miranzo, *Acta Mater.* **2005**, *53*, 3313; b) L. F. Hu, C. A. Wang, Y. Huang, *J. Mater. Sci.* **2010**, *45*, 3242.

[22] E. Litovsky, M. Shapiro, A. Shavit, *J. Am. Ceram. Soc.* **1996**, *79*, 1366.

[23] a) P. Colombo, A. Arcaro, A. Francesconi, D. Pavarin, D. Rondini, S. Debei, *Adv. Eng. Mater.* **2003**, *5*, 802; b) B. S. M. Seeber, U. T. Gonzenbach, L. J. Gauckler, *J. Mater. Res.* **2013**, *28*, 2281.

[24] T. E. G. Alvarez-Arenas, F. R. M. de Espinosa, M. Moner-Girona, E. Rodriguez, A. Roig, E. Molins, *Appl. Phys. Lett.* **2002**, *81*, 1198.

[25] T. Brunet, A. Merlin, B. Mascaro, K. Zimny, J. Leng, O. Poncelet, C. Aristegui, O. Mondain-Monval, *Nat. Mater.* **2015**, *14*, 384.

[26] V. S. Deshpande, N. A. Fleck, M. F. Ashby, *J. Mech. Phys. Solids* **2001**, *49*, 1747.

[27] a) S. Barg, F. M. Perez, N. Ni, P. D. V. Pereira, R. C. Maher, E. Garcia-Tunon, S. Eslava, S. Agnoli, C. Mattevi, E. Saiz, *Nat. Commun.* **2014**, *5*, 4328; b) N. Na, S. Barg, E. Garcia-Tunon, F. Macul Perez, M. Miranda, C. Lu, C. Mattevi, E. Saiz, *Sci. Rep.* **2015**, *5*, 13712; c) L. Qiu, J. Z. Liu, S. L. Y. Chang, Y. Z. Wu, D. Li, *Nat. Commun.* **2012**, *3*, 1241; d) M. A. Worsley, S. O. Kucheyev, J. H. Satcher, A. V. Hamza, T. F. Baumann, *Appl. Phys. Lett.* **2009**, *94*, 073115.

[28] P. Miranda, A. Pajares, E. Saiz, A. P. Tomsia, F. Guiberteau, *J. Biomed. Mater. Res. A* **2007**, *83A*, 646.

[29] K. E. Pappacena, K. T. Faber, H. Wang, W. D. Porter, *J. Am. Ceram. Soc.* **2007**, *90*, 2855.

[30] a) GRANTA CES 2009 EDUPACK, Resource booklet 2: Materials and Process Selection Chart, Granta Design, Cambridge, UK, 2009; b) University of Cambridge, Department of Engineering, Materials Selection and Processing, Materials Information, Materials Selection Charts, http://www-materials.eng.cam.ac.uk/mpsite/interactive_charts, accessed June 1015.

[31] a) M. W. Barsoum, *Fundamentals of Ceramics,* McGraw Hill, New York **1997**; b) W. W. Cai, A. L. Moore, Y. W. Zhu, X. S. Li, S. S. Chen, L. Shi, R. S. Ruoff, *Nano Lett.* **2010**, *10*, 1645; c) R. Menzel, S. Barg, M. Miranda, D. B. Anthony, S. M. Bawaked, M. Mokhtar, S. A. Al-Thabaiti, S. N. Basahel, E. Saiz, M. S. P. Shaffer, *Adv. Funct. Mater.* **2015**, *25*, 28.

[32] S. Deville, E. Saiz, R. K. Nalla, A. P. Tomsia, *Science* **2006**, *311*, 515.

[33] T. E. G. Alvarez-Arenas, *IEEE Trans. Ultrason. Ferr.* **2004**, *51*, 624.

[34] a) T. E. G. Alvarez-Arenas, *Ultrasonics* **2010**, *50*, 104; b) M. D. Farinas, T. E. G. Alvarez-Arenas, *J. Mech. Behav. Biomed. Mater.* **2014**, *39*, 304.